Directional limits on persistent gravitational waves using data from Advanced LIGO's first two observing runs

The LIGO Scientific Collaboration and The Virgo Collaboration
(Dated: July 17, 2019)

We perform an unmodeled search for persistent, directional gravitational wave (GW) sources using data from the first and second observing runs of Advanced LIGO. We do not find evidence for any GW signals. We place limits on the broadband GW flux emitted at 25 Hz from point sources with a power law spectrum at $F_{\alpha,\Theta} < (0.05-25)\times10^{-8}\,\mathrm{erg\,cm^{-2}\,s^{-1}\,Hz^{-1}}$ and the (normalized) energy density spectrum in GWs at 25 Hz from extended sources at $\Omega_\alpha(\Theta) < (0.19-2.89)\times10^{-8}\,\mathrm{sr^{-1}}$ where α is the spectral index of the energy density spectrum. These represent improvements of $2.5-3\times$ over previous limits. We also consider point sources emitting GWs at a single frequency, targeting the directions of Sco X-1, SN 1987A, and the Galactic Center. The best upper limits on the strain amplitude of a potential source in these three directions range from $h_0 < (3.6-4.7)\times10^{-25}$, $1.5\times$ better than previous limits set with the same analysis method. We also report on a marginally significant outlier at 36.06 Hz. This outlier is not consistent with a persistent gravitational-wave source as its significance diminishes when combining all of the available data.

I. INTRODUCTION

The stochastic gravitational wave (GW) background (SGWB) is the superposition of many sources of GWs in the Universe [1]. Anisotropies in the SGWB can be generated by spatially extended sources such as a population of neutron stars in the galactic plane or a nearby galaxy [2, 3], or from perturbations in statistically-isotropic backgrounds formed at cosmological distances such as the compact binary background [4–9] or the background from cosmic strings [10]. Cross-correlation based methods have been used to search for the anisotropic background in previous observing runs [11–14] of the initial and Advanced Laser Interferomter Gravitational-wave Observatory (LIGO) [15], and future searches will incorporate data from the Advanced Virgo [16] detector. Using very similar techniques, one can also search for point sources with an unknown phase evolution, which could include rotating neutron stars in the Galaxy [17, 18]. Since a SGWB search is by nature un-modelled, performing the anisotropic SGWB search allows us to take an eyes-wide-open approach to exploring the GW sky.

In this paper, we present the results of three complementary searches, which probe different types of anisotropy. All of the searches are based on cross-correlation methods; for a review see [19]. A spherical harmonic decomposition (SHD) of the GW power on the sky [12, 20] is optimized to search for extended sources on the sky with a smooth frequency spectrum. The broadband radiometer analysis [17, 18] (BBR) is optimized for detecting resolvable, persistent point-sources emitting GWs across a wide frequency band. Finally, the directed narrowband radiometer (NBR) looks at the frequency spectrum for three astrophysically interesting directions: Scorpius X-1 (Sco X-1) [21, 22], Supernova 1987A (SN 1987A) [23, 24], and the Galactic Center [25, 26]. We do not find a significant detection for any of the searches, and so we place upper limits on the amplitude of the anisotropic SGWB, and on point sources with broad and narrow frequency ranges. Our upper limits improve on the best results from previous runs [11] by approximately a factor of 2.5-3 for the broadband searches and a factor of 1.5 for the narrowband searches. For the narrowband radiometer search, we find a marginally significant outlier in the direction of SN 1987A, when analyzing just the data from LIGO's second observing run (O2). Its significance diminishes, however, when including all of the available data.

II. DATA

We analyze strain data from the first (O1) and second (O2) observing runs of Advanced LIGO's 4 km detectors in Hanford, Washington (H1) and Livingston, Louisiana (L1). The O1 data set used here was collected from 15:00 UTC on 18 September, 2015 to 16:00 UTC on 12 January, 2016, while the O2 data set was collected from 16:00:00 UTC on 30 November, 2016 to 22:00:00 UTC on 25 August, 2017. In O2, linearly coupled noise was removed from the strain time series at H1 and L1 using Wiener filtering [27–31]. The Virgo (V1) detector started to collect data from August 2017 but does not contribute significantly to the sensitivity of SGWB searches in O2, both because its noise level is much higher than the LIGO detectors and because it ran for a much shorter period of time. Therefore, we do not include Virgo in this analysis. We plan, however, to include Virgo in the analysis of data from future observation runs.

Our data processing methods follow the procedure used in O1 [11, 32]. First, we down-sample the strain time series from 16,384 Hz to 4,096 Hz. We then divide the data into 192 s, 50% overlapping, Hann-windowed segments, and apply a cascading 16th order Butterworth digital high-pass filter with a knee frequency of 11 Hz. We compute the cross correlation of coincident 192 s segments at both detectors in the frequency domain, and then coarse-grain to a frequency resolution of 1/32 Hz. Finally, we optimally combine results from those overlapping time segments to produce the final cross-correlation

estimate [33].

In order to account for non-Gaussian features in the data, we remove segments associated with instrumental artifacts and hardware injections used for signal validation [34, 35]. Segments containing known GW signals [36] are also excluded. Finally, we apply a non-stationarity cut (see, e.g., [37]) to eliminate segments where the power spectral density of the noise changes on time scales that are of the same order as the chosen segment length. In total these cuts removed 16% of the data, leading to a total search live-time of 99 days from the O2 run. For our results where we combine data between the O1 and O2 observing runs we have a total search livetime of 129 days. In addition, frequency bins associated with known instrumental artifacts are removed [38]. These frequency domain cuts discarded 4% of the most sensitive frequency band for the BBR and SHD searches and 15% of the observing band for the NBR search. The subtraction of linearly coupled noise did not introduce any new frequency domain cuts.

The broadband searches integrate over frequencies between 20 and 500 Hz. This range accounts for more than 99% of the sensitivity for the power law spectral models that we use (see Table 1 of [39]). The narrowband analysis searches over the frequency band from 20 to 1726 Hz using frequency bins of various sizes depending upon frequency and sky direction. The lower edge of this range is chosen because of increased noise and non-stationarity at lower frequencies, while the upper edge of the range is a product of the filter used to resample the data from 16,384 Hz to 4,096 Hz.

III. METHODS

The anisotropic SGWB background can be defined in terms of the dimensionless energy density $\Omega_{\rm gw}(f,\Theta)$ per unit frequency f and solid angle Θ,

$$\Omega_{\rm gw}(f,\Theta) = \frac{f}{\rho_c}\frac{{\rm d}^3\rho_{GW}}{{\rm d}f{\rm d}^2\Theta}, \tag{1}$$

where $\rho_c = 3H_0^2c^2/(8\pi G)$ is the critical energy density needed to have a spatially flat Universe. We take the Hubble constant to be $H_0 = 67.9\,{\rm km\,s^{-1}\,Mpc^{-1}}$ [40]. Following past analyses, we assume that we can factorize $\Omega_{\rm gw}$ into frequency and sky-direction dependent terms,

$$\Omega_{\rm gw}(f,\Theta) = \frac{2\pi^2}{3H_0^2}f^3H(f)\mathcal{P}(\Theta). \tag{2}$$

This quantity has units of the dimensionless energy density parameter per steradian. For the radiometer searches it is useful to define a different representation in terms of energy flux,

$$\mathcal{F}(f,\Theta) = \frac{c^3\pi}{4G}f^2H(f)\mathcal{P}(\Theta), \tag{3}$$

which has units of ${\rm erg\,cm^{-2}\,s^{-1}\,Hz^{-1}\,sr^{-1}}$, where c is the speed of light and G is Newton's gravitational constant.

We divide the searches into the *broadband* searches (SHD and BBR), which produce sky maps where the flux has been integrated over a broad range of frequencies, and the *narrowband* search (NBR), which looks at the strain amplitude spectrum in a fixed sky direction. For the broadband searches, we typically assume that the energy spectrum has a power law form, $H(f) = (f/f_{\rm ref})^{\alpha-3}$, where $\alpha = \{0, 2/3, 3\}$ describes a range of astrophysical and cosmological models [11], and $f_{\rm ref}$ is a reference frequency which we take to be 25 Hz, as in [11]. The SHD search looks for sources with a large angular extent. We express the results in terms of the spherical harmonic decomposition of $\Omega_{\rm gw}(f,\Theta)$ assuming a power-law in frequency of spectral index α. We then report the energy density in each direction at a reference frequency of 25 Hz, denoted by $\Omega_\alpha(\Theta)$.

For the BBR search, we assume that the angular distribution of the power is localized in a $1\,{\rm deg}^2$ pixel, $\mathcal{P}(\Theta) = \mathcal{P}_{\Theta_0}\delta^2(\Theta,\Theta_0)$. The results of the BBR are then given in terms of the quantity F_{α,Θ_0}, which is the flux evaluated at the reference frequency of 25 Hz, assuming a power law, after integrating over solid angle. The explicit definitions of F_{α,Θ_0} and $\Omega_\alpha(\Theta)$ are given in the Technical Supplement.

Finally, the NBR search does not integrate over frequency, and attempts to measure the strain amplitude, h_0, of a putative monochromatic source in each frequency bin independently. This includes combining adjacent 0.031 Hz frequency bins together to account for the Doppler modulation due to the motion of the Earth around the solar system barycenter and any binary motion of the source itself [11].

The full description of the methods used to search for an anisotropic SGWB is presented in the Technical Supplement and in the paper describing the analysis of the Advanced LIGO O1 data. We follow the notation presented in that Letter [11].

The searches all generally start by estimating the dirty map X_ν, and its corresponding covariance matrix $\Gamma_{\mu\nu}$, referred to here as the Fisher matrix [11, 20, 41]. The dirty map represents an estimate of the GW power as seen through the detector's beam matrix.

Given the Fisher matrix $\Gamma^I_{\mu\nu}$ and dirty map X^I_ν, where I labels the observing run, we can form a combined Fisher matrix and dirty map by summing the results from the two runs, O1 and O2 [19]

$$\begin{aligned}\Gamma_{\mu\nu} &= \Gamma^{(\rm O1)}_{\mu\nu} + \Gamma^{(\rm O2)}_{\mu\nu},\\ X_\mu &= X^{(\rm O1)}_\mu + X^{(\rm O2)}_\mu.\end{aligned} \tag{4}$$

From the combined Fisher matrix and dirty map, we can construct estimators of the power on the sky via:

$$\hat{\mathcal{P}}_\mu = \sum_\nu \left(\Gamma^{-1}_{\rm R}\right)_{\mu\nu} X_\nu\,. \tag{5}$$

In the above equations, μ, ν label either pixels (i.e., directions on the sky) or spherical harmonic components—i.e.,

			All-sky (broadband) Results					
			Max SNR (% p-value)		Upper limit ranges		O1 Upper limit ranges	
α	$\Omega_{\rm gw}$	$H(f)$	BBR	SHD	BBR ($\times 10^{-8}$)	SHD ($\times 10^{-8}$)	BBR ($\times 10^{-8}$)	SHD ($\times 10^{-8}$)
0	constant	$\propto f^{-3}$	3.09 (9)	2.98 (9)	4.4 – 25	0.78 – 2.90	15 – 65	3.2 – 8.7
2/3	$\propto f^{2/3}$	$\propto f^{-7/3}$	3.09 (20)	2.61 (31)	2.3 – 14	0.64 –2.47	7.9 – 39	2.5 – 6.7
3	$\propto f^{3}$	constant	3.27 (66)	3.57 (27)	0.05 – 0.33	0.19 – 1.1	0.14 – 1.1	0.5 – 3.1

TABLE I. Search information for BBR and SHD. On the left side of the table we show the value of the power-law spectral index, α, and the scaling of $\Omega_{\rm gw}$ and $H(f)$ with frequency. To the right we show results for the broadband radiometer (BBR) and spherical harmonic decomposition (SHD) searches for the combined O1 and O2 analysis, as well as the results from O1 for comparison. We show the maximum SNR across all sky positions for each spectral index, as well as an estimated p-value. We also show the range of 95% upper limits on energy flux set by the BBR search across the whole sky [erg cm^{-2} s^{-1} Hz^{-1}] and the SHD range of upper limits on normalized energy density across the whole sky [sr^{-1}]. These limits use data from both O1 and O2. The median improvement across the sky compared to limits set in O1 is 2.6-2.7 for the BBR search and 2.8-3 for the SHD search, depending on power-law spectral index.

$\mu \equiv (lm)$, depending on which basis is used to represent the sky maps. The subscript 'R' on the Fisher matrix means that regularization has been applied (e.g., singular value decomposition) in order to perform the matrix inversion [11].

We can also construct an estimate of the angular power spectrum, C_l, for the SGWB from the estimate of the spherical harmonics coefficients, $\hat{\mathcal{P}}_{lm}$. The C_l's describe the angular scale of the structure found in the clean maps [20]

$$\hat{C}_l = \left(\frac{2\pi^2 f_{\rm ref}^3}{3H_0^2}\right)^2 \frac{1}{1+2l} \sum_{m=-l}^{l} \left[|\hat{\mathcal{P}}_{lm}|^2 - (\Gamma_{\rm R}^{-1})_{lm,lm}\right]. \tag{6}$$

We have also used theoretical models for the SGWB from compact binaries [4] and from Nambu-Goto cosmic strings [10] to check our assumption that the SGWB energy density $\Omega_{\rm gw}(f,\Theta)$ can be factorised into a spectral shape term and an angular power term. We find that both models predict C_l's that follow the appropriate frequency power laws ($\alpha = 2/3$ for compact binaries and $\alpha = 0$ for cosmic strings) across the frequency range in which the LIGO stochastic searches are most sensitive, thereby supporting this assumption (see also [42]).

IV. RESULTS

A. Broadband radiometer and spherical harmonic decomposition results

The sky maps for the BBR search are shown in Figure 1, and for the SHD search in Figure 2. Converting maps from the spherical harmonics basis (i.e. $\mu = (lm)$) to the pixel basis is discussed in detail in [20]. Each column indicates a different value of the spectral index, α. The top row shows a map of the signal-to-noise ratio (SNR) for each sky direction. The SNR sky maps are consistent with Gaussian noise (see the p-values given in Table I). Consequently, we place upper limits on the amount of GW power in each pixel using the methods outlined in [43]. The bottom rows of Figures 1 and 2 show maps of these upper limits for the BBR and SHD analyses, respectively. The minimum and maximum 95% confidence upper limits across all pixels for both the BBR and SHD searches are shown in Table I. These limits represent a median improvement across the sky of 2.6-2.7 for the BBR search and 2.8-3 for the SHD search, depending on the power-law spectral index, α.

B. Limits on angular power spectra

We also use the maps from the SHD analysis to set upper limits on the angular power spectrum components, C_l. The upper limits are shown for three spectral indices in Figure 3. The upper limit for $\alpha = 2/3$ can be compared with theoretical predictions in the literature for the SGWB from compact binaries [4, 6, 44]. In particular, the calculation in Refs. [4, 44] gives $C_l^{1/2} \approx 3\times10^{-11}$ sr^{-1} for $1 \leq l \leq 4$ (the calculation in Ref. [6] gives values that are $\sim 10\times$ smaller). Similarly, the upper limit for $\alpha = 0$ can be compared with predictions for the SGWB from Nambu-Goto cosmic strings in Ref. [10], using the same models for the string network as in Ref. [45]. Assuming the isotropic component of the cosmic string SGWB is consistent with the upper limits set by LIGO's second observing run [39], the dipole ($l = 1$) can be as large as $C_1^{1/2} \approx 10^{-10}$ sr^{-1}, though the values for higher multipoles $l > 1$ are many orders of magnitude smaller. These predictions are therefore consistent with the upper limits obtained here, and present an important target for future observing runs.

Looking forward towards the prospect of detection, it is important to note that the finite sampling of the galaxy distribution and the compact binary coalescence event rate induces a shot noise in the anisotropies of the astrophysical GW background. As it has been recently shown [46] this shot noise leads to a scale-invariant bias term in the angular power spectrum C_l and it scales with observing time. Such a bias will dominate over the true cosmological power spectrum, which to be recovered will need either sufficiently long observing times or subtraction of the foreground.

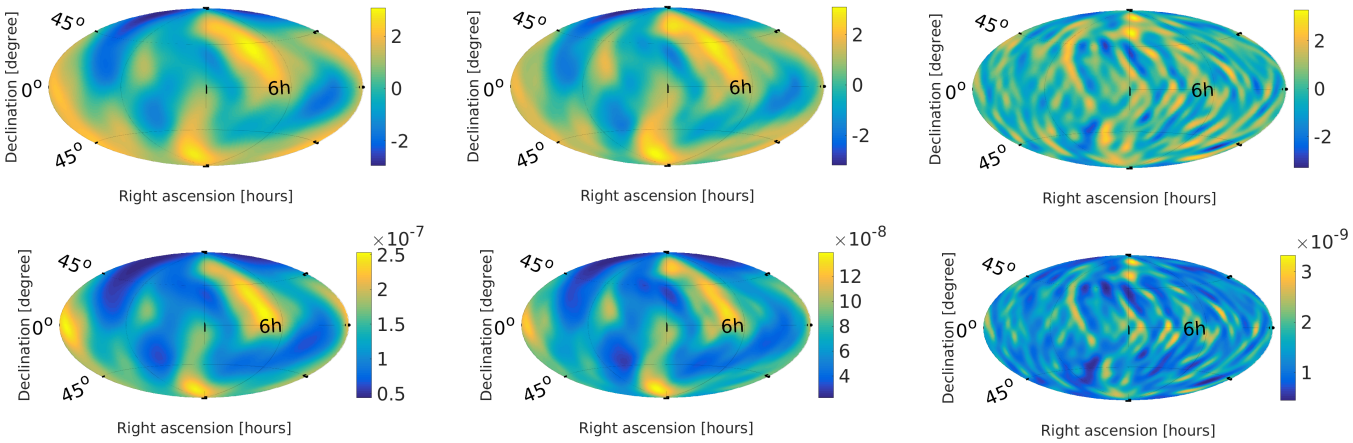

FIG. 1. Broadband radiometer maps illustrating a search for point-like sources. The top row shows maps of SNR, while the bottom row shows maps of the upper limits at 95% confidence on energy flux F_{α,Θ_0} [erg cm^{-2} s^{-1} Hz^{-1}]. Three different power-law indices, $\alpha = 0$, 2/3 and 3, are represented from left to right. The p-values associated with the maximum SNR are (from left to right) $p = 9\%$, $p = 20\%$, $p = 66\%$ (see Table I).

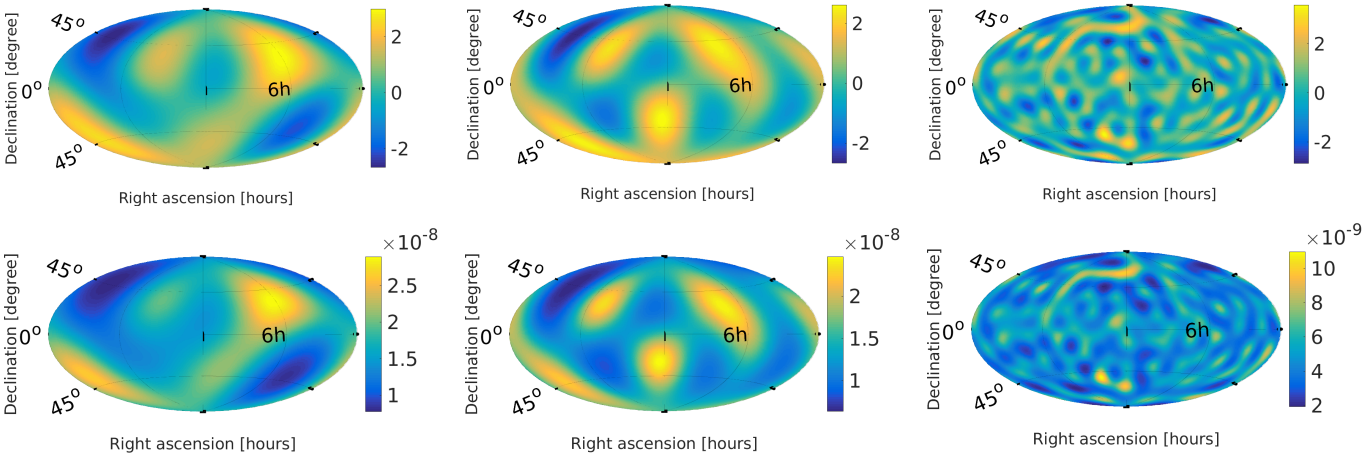

FIG. 2. All-sky maps reconstructed from a spherical harmonic decomposition. This search is optimized for extended sources, and the plots above show SNR (top) and upper limits at 95% confidence on the energy density of the SGWB Ω_α [sr^{-1}] (bottom). Results for three different power-law spectral indices, $\alpha = 0$, 2/3 and 3 are shown from left to right. These three different sets of maps have an $l_{\rm max}$ of 3, 4, and 16 respectively. The p-values associated with the maximum SNR are (from left to right) $p = 9\%$, $p = 31\%$, $p = 27\%$ (see Table I).

C. Narrowband radiometer results

The narrowband radiometer search estimates the strain amplitude, h_0, of a potential source of GWs in three different directions. The maximum SNR across the frequency band and an estimate of the significance of that SNR for each direction are shown in Table II. The uncertainty on the frequency for the SNR reported in Table II is a reflection of the original (uncombined) frequency bin width. The ephemeris for Scorpius X-1 has been updated since the publication of [11], and so the search presented below assumes a projected semi-major axis, a_0, in the center of the range presented by [47].

In the direction of Sco X-1 and the Galactic Center, the maximum SNR is consistent with what one expects from Gaussian noise. In the direction of SN 1987A, there is a frequency bin with a 1-sided, single-direction p-value 1.7% at 181.8 Hz. This p-value includes a trials factor for the number of frequency bins in the analysis. Under the assumption that we search over three independent directions, an extra trials factor would be applied and this p-value rises to 5%. Therefore, we find no compelling evidence for GWs from the analysis that combines frequency bins together. We set 95% upper limits on the strain amplitude of a putative sinusoidal gravitational wave signal, h_0, in each individual frequency bin, taking into account any Doppler modulation in the signal as well as marginalizing over inclination angle and polarization angle of the source [11]. These limits, along with the 1σ sensitivity of the search, are shown in Figure 4. To avoid

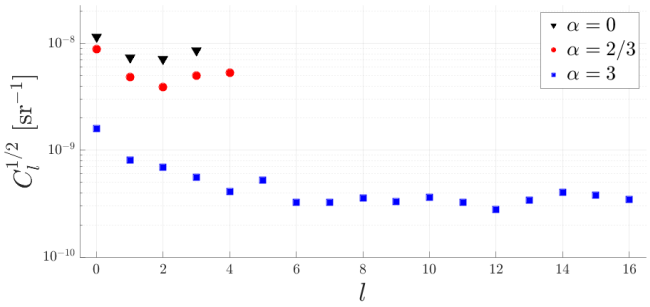

FIG. 3. Upper limits on C_l's at 95% confidence for the SHD analyses for $\alpha = 0$ (top, black triangles), $\alpha = 2/3$ (middle, red circles) and $\alpha = 3$ (bottom, blue squares). These represent an improvement in upper limits over O1 of 2.5 – 3 depending on spectral index, α, and l.

reporting our best limits from downward fluctuations of noise, we take a running median over each 1 Hz frequency band and report the best limit on h_0 and the frequency band of that limit in Table II.

The best limits on Sco-X1 set in this paper are higher than the best limit set in O1 using a model-based cross-correlation method [21], and are now lower than those set using hidden Markov model tracking [22]. The torque-balance limit, set by assuming that torque due to accretion is equal to the braking torque due to GW emission, is still around a factor of 5 lower than the limits set in this paper. The best limits on h_0 in the direction of the Galactic Center and SN 1987A are generally higher than previous modeled searches for isolated neutron stars [23, 25, 26, 48, 49] in the frequency bands where those analyses overlap with the one presented here. This search spans a wider frequency band (20-1726 Hz) than any one of those individual analyses. It is important to note that the search presented in this paper is inherently unmodeled, meaning it makes no assumption about the phase evolution of a potential signal past timescales of 192 s.

V. OUTLIER AT 36.06 HZ IN THE O2 DATA

In the process of performing the narrowband radiometer search, a natural intermediate step of the analysis is to look directly at the 0.03125 Hz bins for the O2 data, before combining with O1 and before combining over adjacent bins to account for Doppler modulation. We call these "sub-bins". For this intermediate data product, the maximum SNRs for the Galactic Center, Sco X-1, and SN 1987A are 4.6, 4.3, and 5.3, respectively. These first two values correspond to p-values greater than 5%, consistent with Gaussian noise. But for SN 1987A, the maximum SNR of 5.3 at 36.0625 Hz has a corresponding p-value of 0.27%, or 3σ, which is marginally significant.

Assuming that the maximum SNR is due to a pulsar which is spinning down due to GW emission, we can relate the observed strain $h_0 = 7.3\times10^{-25}$ (assuming circular polarization) at $f = 36.06$ Hz to other parameters describing the pulsar:

$$h_0 = \frac{4\pi G}{c^4}\frac{\epsilon I_z f^2}{r}, \quad \dot{f} = -\frac{G}{5\pi c^5}\epsilon^2 I_z (2\pi f)^5. \qquad (7)$$

We use a fiducial value for the moment of inertia $I_z = 10^{39}$ kg $\cdot$ m^2. If the source is associated with SN 1987A, then the distance to Earth is approximately $r = 51$ kpc [50, 51], leading to an ellipticity $\epsilon = 3\times10^{-2}$ and spin down $\dot{f} = -7.7\times10^{-8}$ Hz/s. But this value of the spin down parameter is inconsistent with the fact that the signal is seen in only one frequency bin. For the signal to remain in a single frequency bin, it either needs to have some balancing torque, perhaps from accretion [52], or the signal would need to be at $r \lesssim 1$ kpc (corresponding to $\dot{f} = -2.9\times10^{-11}$ Hz/s). In the latter case, the ellipticity $\epsilon = 5\times10^{-4}$ is still much larger than that predicted for typical pulsars. An ellipticity this large is unlikely to be caused by elastic deformations [53], but could in principle be caused by large internal magnetic fields [54–56], especially if the protons form a type II superconductor [57]. It is important to note that an all-sky search for continuous GWs from isolated systems has set limits more stringent than our estimate of h_0 for this outlier [49].

Using the techniques described in [38], we have not been able to identify a coherent instrumental witness channel that would explain this large SNR. But the fact that the sky direction of the maximum SNR is close to the equatorial pole is consistent with the behavior of instrumental noise lines, since the equatorial poles have no sidereal-time modulation. The signal appears to turn on during O2, with the SNR exceeding 1 on March 13th, 2017, as shown in Figure 5. In addition, the signal does not exhibit any significant short-term non-stationarity, indicating that this outlier is not generated from a small number of mis-behaved time chunks with large SNRs. The turn-on feature of the cumulative SNR is not evidence of a real signal, however, as we have performed simulations of Gaussian noise conditioned on getting a maximum SNR ≥ 5, and have found examples where a turn-on like this can be produced. In addition, upon combining O2 and O1 data together, the SNR of this frequency bin is reduced to 4.7, which corresponds to a p-value of 10%, which is consistent with noise.

VI. CONCLUSIONS

We have placed upper limits on the anisotropic SGWB using three complementary methods. In each case we do not find conclusive evidence for a GW signal, and so we place upper limits by combining data from Advanced LIGO's first and second observing runs. A marginal outlier at a frequency of 36.06 Hz was seen by the narrowband radiometer search in O2 in the direction of SN 1987A; however it does not appear in the combined

Narrowband Radiometer Results

Direction	Max SNR	p-value (%)	Frequency (Hz) ($\pm$ 0.016 Hz)	Best UL ($\times 10^{-25}$)	Frequency band (Hz)
Sco X-1	4.80	4.5	1602.09	4.2	$183.6 - 184.6$
SN 1987A	4.95	1.7	181.81	3.6	$247.75 - 248.75$
Galactic Center	3.80	98	20.28	4.7	$156.8 - 157.8$

TABLE II. Results for the narrowband radiometer search. We give the maximum SNR, corresponding p-value, and the frequency bin of the maxmum SNR for each direction in which we searched. We also give the best 95% GW strain upper limits achieved, and the corresponding frequency band, for all three sky locations. The best upper limits are taken as the median of the most sensitive 1 Hz band.

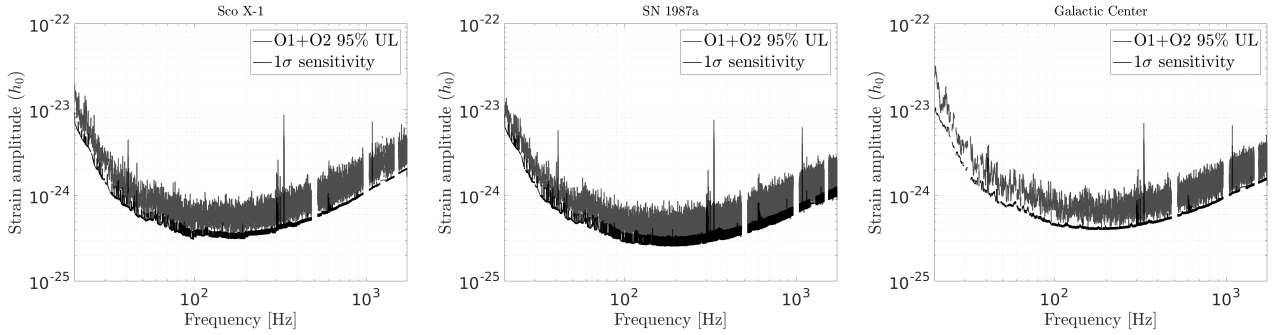

FIG. 4. Upper limit spectra using data from O1 and O2 on the dimensionless strain amplitude, h_0, at the 95% level for the narrowband radiometer search are indicated by the gray bands for Sco X-1 (left), SN 1987A (middle) and the Galactic Center (right). The dark black line indicates the 1σ sensitivity of the search in all three directions. The large spikes are the result of the calibration lines injected into the detector and suspension-wire resonances for various optical elements throughout the instruments.

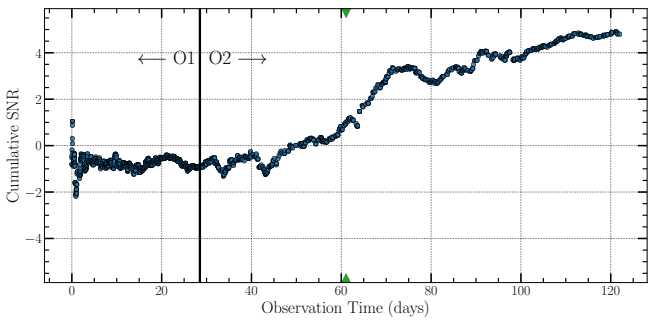

FIG. 5. The accumulation of SNR as a function of time for SN 1987a, including both O1 and O2 data. The curve shows the observed cumulative SNR in the 36.06 Hz frequency bin. The green arrows indicate the point where the SNR moves above 1 for the remainder of the available observation time.

O1+O2 data and is not consistent with a persistent signal. We will continue to monitor this particular frequency bin during the next observing run, taking advantage of the greater confidence that comes with increased observation periods and more sensitive detectors.

In the future, the anisotropic searches will include data from Advanced Virgo as well, and can be used to study specific astrophysical models. Additionally, new algorithms can take advantage of folded data to produce a wider search of every frequency and sky position [58–61].

VII. ACKNOWLEDGEMENTS

The authors gratefully acknowledge the support of the United States National Science Foundation (NSF) for the construction and operation of the LIGO Laboratory and Advanced LIGO as well as the Science and Technology Facilities Council (STFC) of the United Kingdom, the Max-Planck-Society (MPS), and the State of Niedersachsen/Germany for support of the construction of Advanced LIGO and construction and operation of the GEO600 detector. Additional support for Advanced LIGO was provided by the Australian Research Council. The authors gratefully acknowledge the Italian Istituto Nazionale di Fisica Nucleare (INFN), the French Centre National de la Recherche Scientifique (CNRS) and the Foundation for Fundamental Research on Matter supported by the Netherlands Organisation for Scientific Research, for the construction and operation of the Virgo detector and the creation and support of the EGO consortium. The authors also gratefully acknowledge research support from these agencies as well as by the Council of Scientific and Industrial Research of India, the Department of Science and Technology, India, the Science & Engineering Research Board (SERB), India, the Ministry of Human Resource Development, India, the Spanish Agencia Estatal de Investigación, the Vicepresidència i Conselleria d'Innovació, Recerca i Turisme and the Conselleria d'Educació i Universitat del Govern de les Illes Balears, the Conselleria d'Educació, Investigació, Cultura i Es-

port de la Generalitat Valenciana, the National Science Centre of Poland, the Swiss National Science Foundation (SNSF), the Russian Foundation for Basic Research, the Russian Science Foundation, the European Commission, the European Regional Development Funds (ERDF), the Royal Society, the Scottish Funding Council, the Scottish Universities Physics Alliance, the Hungarian Scientific Research Fund (OTKA), the Lyon Institute of Origins (LIO), the Paris Île-de-France Region, the National Research, Development and Innovation Office Hungary (NKFIH), the National Research Foundation of Korea, Industry Canada and the Province of Ontario through the Ministry of Economic Development and Innovation, the Natural Science and Engineering Research Council Canada, the Canadian Institute for Advanced Research, the Brazilian Ministry of Science, Technology, Innovations, and Communications, the International Center for Theoretical Physics South American Institute for Fundamental Research (ICTP-SAIFR), the Research Grants Council of Hong Kong, the National Natural Science Foundation of China (NSFC), the Leverhulme Trust, the Research Corporation, the Ministry of Science and Technology (MOST), Taiwan and the Kavli Foundation. The authors gratefully acknowledge the support of the NSF, STFC, MPS, INFN, CNRS and the State of Niedersachsen/Germany for provision of computational resources.

The LIGO Scientific Collaboration and Virgo Collaboration

B. P. Abbott,[1] R. Abbott,[1] T. D. Abbott,[2] S. Abraham,[3] F. Acernese,[4,5] K. Ackley,[6] C. Adams,[7] R. X. Adhikari,[1] V. B. Adya,[8,9] C. Affeldt,[8,9] M. Agathos,[10] K. Agatsuma,[11] N. Aggarwal,[12] O. D. Aguiar,[13] L. Aiello,[14,15] A. Ain,[3] P. Ajith,[16] G. Allen,[17] A. Allocca,[18,19] M. A. Aloy,[20] P. A. Altin,[21] A. Amato,[22] A. Ananyeva,[1] S. B. Anderson,[1] W. G. Anderson,[23] S. V. Angelova,[24] S. Antier,[25] S. Appert,[1] K. Arai,[1] M. C. Araya,[1] J. S. Areeda,[26] M. Arène,[27] N. Arnaud,[25,28] S. Ascenzi,[29,30] G. Ashton,[6] S. M. Aston,[7] P. Astone,[31] F. Aubin,[32] P. Aufmuth,[9] K. AultONeal,[33] C. Austin,[2] V. Avendano,[34] A. Avila-Alvarez,[26] S. Babak,[35,27] P. Bacon,[27] F. Badaracco,[14,15] M. K. M. Bader,[36] S. Bae,[37] P. T. Baker,[38] F. Baldaccini,[39,40] G. Ballardin,[28] S. W. Ballmer,[41] S. Banagiri,[42] J. C. Barayoga,[1] S. E. Barclay,[43] B. C. Barish,[1] D. Barker,[44] K. Barkett,[45] S. Barnum,[12] F. Barone,[4,5] B. Barr,[43] L. Barsotti,[12] M. Barsuglia,[27] D. Barta,[46] J. Bartlett,[44] I. Bartos,[47] R. Bassiri,[48] A. Basti,[18,19] M. Bawaj,[49,40] J. C. Bayley,[43] M. Bazzan,[50,51] B. Bécsy,[52] M. Bejger,[27,53] I. Belahcene,[25] A. S. Bell,[43] D. Beniwal,[54] B. K. Berger,[48] G. Bergmann,[8,9] S. Bernuzzi,[55,56] J. J. Bero,[57] C. P. L. Berry,[58] D. Bersanetti,[59] A. Bertolini,[36] J. Betzwieser,[7] R. Bhandare,[60] J. Bidler,[26] I. A. Bilenko,[61] S. A. Bilgili,[38] G. Billingsley,[1] J. Birch,[7] R. Birney,[24] O. Birnholtz,[57] S. Biscans,[1,12] S. Biscoveanu,[6] A. Bisht,[9] M. Bitossi,[28,19] M. A. Bizouard,[25] J. K. Blackburn,[1] C. D. Blair,[7] D. G. Blair,[62] R. M. Blair,[44] S. Bloemen,[63] N. Bode,[8,9] M. Boer,[64] Y. Boetzel,[65] G. Bogaert,[64] F. Bondu,[66] E. Bonilla,[48] R. Bonnand,[32] P. Booker,[8,9] B. A. Boom,[36] C. D. Booth,[67] R. Bork,[1] V. Boschi,[28] S. Bose,[68,3] K. Bossie,[7] V. Bossilkov,[62] J. Bosveld,[62] Y. Bouffanais,[27] A. Bozzi,[28] C. Bradaschia,[19] P. R. Brady,[23] A. Bramley,[7] M. Branchesi,[14,15] J. E. Brau,[69] T. Briant,[70] J. H. Briggs,[43] F. Brighenti,[71,72] A. Brillet,[64] M. Brinkmann,[8,9] V. Brisson,[25,*] P. Brockill,[23] A. F. Brooks,[1] D. D. Brown,[54] S. Brunett,[1] A. Buikema,[12] T. Bulik,[73] H. J. Bulten,[74,36] A. Buonanno,[35,75] D. Buskulic,[32] C. Buy,[27] R. L. Byer,[48] M. Cabero,[8,9] L. Cadonati,[76] G. Cagnoli,[22,77] C. Cahillane,[1] J. Calderón Bustillo,[6] T. A. Callister,[1] E. Calloni,[78,5] J. B. Camp,[79] W. A. Campbell,[6] M. Canepa,[80,59] K. C. Cannon,[81] H. Cao,[54] J. Cao,[82] E. Capocasa,[27] F. Carbognani,[28] S. Caride,[83] M. F. Carney,[58] G. Carullo,[18] J. Casanueva Diaz,[19] C. Casentini,[29,30] S. Caudill,[36] M. Cavaglià,[84] F. Cavalier,[25] R. Cavalieri,[28] G. Cella,[19] P. Cerdá-Durán,[20] G. Cerretani,[18,19] E. Cesarini,[85,30] O. Chaibi,[64] K. Chakravarti,[3] S. J. Chamberlin,[86] M. Chan,[43] S. Chao,[87] P. Charlton,[88] E. A. Chase,[58] E. Chassande-Mottin,[27] D. Chatterjee,[23] M. Chaturvedi,[60] B. D. Cheeseboro,[38] H. Y. Chen,[89] X. Chen,[62] Y. Chen,[45] H.-P. Cheng,[47] C. K. Cheong,[90] H. Y. Chia,[47] A. Chincarini,[59] A. Chiummo,[28] G. Cho,[91] H. S. Cho,[92] M. Cho,[75] N. Christensen,[64,93] Q. Chu,[62] S. Chua,[70] K. W. Chung,[90] S. Chung,[62] G. Ciani,[50,51] A. A. Ciobanu,[54] R. Ciolfi,[94,95] F. Cipriano,[64] A. Cirone,[80,59] F. Clara,[44] J. A. Clark,[76] P. Clearwater,[96] F. Cleva,[64] C. Cocchieri,[84] E. Coccia,[14,15] P.-F. Cohadon,[70] D. Cohen,[25] R. Colgan,[97] M. Colleoni,[98] C. G. Collette,[99] C. Collins,[11] L. R. Cominsky,[100] M. Constancio Jr.,[13] L. Conti,[51] S. J. Cooper,[11] P. Corban,[7] T. R. Corbitt,[2] I. Cordero-Carrión,[101] K. R. Corley,[97] N. Cornish,[52] A. Corsi,[83] S. Cortese,[28] C. A. Costa,[13] R. Cotesta,[35] M. W. Coughlin,[1] S. B. Coughlin,[67,58] J.-P. Coulon,[64] S. T. Countryman,[97] P. Couvares,[1] P. B. Covas,[98] E. E. Cowan,[76] D. M. Coward,[62] M. J. Cowart,[7] D. C. Coyne,[1] R. Coyne,[102] J. D. E. Creighton,[23] T. D. Creighton,[103] J. Cripe,[2] M. Croquette,[70] S. G. Crowder,[104] T. J. Cullen,[2] A. Cumming,[43] L. Cunningham,[43] E. Cuoco,[28] T. Dal Canton,[79] G. Dálya,[105] S. L. Danilishin,[8,9] S. D'Antonio,[30]

K. Danzmann,[9,8] A. Dasgupta,[106] C. F. Da Silva Costa,[47] L. E. H. Datrier,[43] V. Dattilo,[28] I. Dave,[60] M. Davier,[25] D. Davis,[41] E. J. Daw,[107] D. DeBra,[48] M. Deenadayalan,[3] J. Degallaix,[22] M. De Laurentis,[78,5] S. Deléglise,[70] W. Del Pozzo,[18,19] L. M. DeMarchi,[58] N. Demos,[12] T. Dent,[8,9,108] R. De Pietri,[109,56] J. Derby,[26] R. De Rosa,[78,5] C. De Rossi,[22,28] R. DeSalvo,[110] O. de Varona,[8,9] S. Dhurandhar,[3] M. C. Díaz,[103] T. Dietrich,[36] L. Di Fiore,[5] M. Di Giovanni,[111,95] T. Di Girolamo,[78,5] A. Di Lieto,[18,19] B. Ding,[99] S. Di Pace,[112,31] I. Di Palma,[112,31] F. Di Renzo,[18,19] A. Dmitriev,[11] Z. Doctor,[89] F. Donovan,[12] K. L. Dooley,[67,84] S. Doravari,[8,9] I. Dorrington,[67] T. P. Downes,[23] M. Drago,[14,15] J. C. Driggers,[44] Z. Du,[82] J.-G. Ducoin,[25] P. Dupej,[43] I. Dvorkin,[35] S. E. Dwyer,[44] P. J. Easter,[6] T. B. Edo,[107] M. C. Edwards,[93] A. Effler,[7] P. Ehrens,[1] J. Eichholz,[1] S. S. Eikenberry,[47] M. Eisenmann,[32] R. A. Eisenstein,[12] R. C. Essick,[89] H. Estelles,[98] D. Estevez,[32] Z. B. Etienne,[38] T. Etzel,[1] M. Evans,[12] T. M. Evans,[7] V. Fafone,[29,30,14] H. Fair,[41] S. Fairhurst,[67] X. Fan,[82] S. Farinon,[59] B. Farr,[69] W. M. Farr,[11] E. J. Fauchon-Jones,[67] M. Favata,[34] M. Fays,[107] M. Fazio,[113] C. Fee,[114] J. Feicht,[1] M. M. Fejer,[48] F. Feng,[27] A. Fernandez-Galiana,[12] I. Ferrante,[18,19] E. C. Ferreira,[13] T. A. Ferreira,[13] F. Ferrini,[28] F. Fidecaro,[18,19] I. Fiori,[28] D. Fiorucci,[27] M. Fishbach,[89] R. P. Fisher,[41,115] J. M. Fishner,[12] M. Fitz-Axen,[42] R. Flaminio,[32,116] M. Fletcher,[43] E. Flynn,[26] H. Fong,[117] J. A. Font,[20,118] P. W. F. Forsyth,[21] J.-D. Fournier,[64] S. Frasca,[112,31] F. Frasconi,[19] Z. Frei,[105] A. Freise,[11] R. Frey,[69] V. Frey,[25] P. Fritschel,[12] V. V. Frolov,[7] P. Fulda,[47] M. Fyffe,[7] H. A. Gabbard,[43] B. U. Gadre,[3] S. M. Gaebel,[11] J. R. Gair,[119] L. Gammaitoni,[39] M. R. Ganija,[54] S. G. Gaonkar,[3] A. Garcia,[26] C. García-Quirós,[98] F. Garufi,[78,5] B. Gateley,[44] S. Gaudio,[33] G. Gaur,[120] V. Gayathri,[121] G. Gemme,[59] E. Genin,[28] A. Gennai,[19] D. George,[17] J. George,[60] L. Gergely,[122] V. Germain,[32] S. Ghonge,[76] Abhirup Ghosh,[16] Archisman Ghosh,[36] S. Ghosh,[23] B. Giacomazzo,[111,95] J. A. Giaime,[2,7] K. D. Giardina,[7] A. Giazotto,[19,†] K. Gill,[33] G. Giordano,[4,5] L. Glover,[110] P. Godwin,[86] E. Goetz,[44] R. Goetz,[47] B. Goncharov,[6] G. González,[2] J. M. Gonzalez Castro,[18,19] A. Gopakumar,[123] M. L. Gorodetsky,[61] S. E. Gossan,[1] M. Gosselin,[28] R. Gouaty,[32] A. Grado,[124,5] C. Graef,[43] M. Granata,[22] A. Grant,[43] S. Gras,[12] P. Grassia,[1] C. Gray,[44] R. Gray,[43] G. Greco,[71,72] A. C. Green,[11,47] R. Green,[67] E. M. Gretarsson,[33] P. Groot,[63] H. Grote,[67] S. Grunewald,[35] P. Gruning,[25] G. M. Guidi,[71,72] H. K. Gulati,[106] Y. Guo,[36] A. Gupta,[86] M. K. Gupta,[106] E. K. Gustafson,[1] R. Gustafson,[125] L. Haegel,[98] O. Halim,[15,14] B. R. Hall,[68] E. D. Hall,[12] E. Z. Hamilton,[67] G. Hammond,[43] M. Haney,[65] M. M. Hanke,[8,9] J. Hanks,[44] C. Hanna,[86] O. A. Hannuksela,[90] J. Hanson,[7] T. Hardwick,[2] K. Haris,[16] J. Harms,[14,15] G. M. Harry,[126] I. W. Harry,[35] C.-J. Haster,[117] K. Haughian,[43] F. J. Hayes,[43] J. Healy,[57] A. Heidmann,[70] M. C. Heintze,[7] H. Heitmann,[64] P. Hello,[25] G. Hemming,[28] M. Hendry,[43] I. S. Heng,[43] J. Hennig,[8,9] A. W. Heptonstall,[1] Francisco Hernandez Vivanco,[6] M. Heurs,[8,9] S. Hild,[43] T. Hinderer,[127,36,128] D. Hoak,[28] S. Hochheim,[8,9] D. Hofman,[22] A. M. Holgado,[17] N. A. Holland,[21] K. Holt,[7] D. E. Holz,[89] P. Hopkins,[67] C. Horst,[23] J. Hough,[43] E. J. Howell,[62] C. G. Hoy,[67] A. Hreibi,[64] E. A. Huerta,[17] D. Huet,[25] B. Hughey,[33] M. Hulko,[1] S. Husa,[98] S. H. Huttner,[43] T. Huynh-Dinh,[7] B. Idzkowski,[73] A. Iess,[29,30] C. Ingram,[54] R. Inta,[83] G. Intini,[112,31] B. Irwin,[114] H. N. Isa,[43] J.-M. Isac,[70] M. Isi,[1] B. R. Iyer,[16] K. Izumi,[44] T. Jacqmin,[70] S. J. Jadhav,[129] K. Jani,[76] N. N. Janthalur,[129] P. Jaranowski,[130] A. C. Jenkins,[131] J. Jiang,[47] D. S. Johnson,[17] A. W. Jones,[11] D. I. Jones,[132] R. Jones,[43] R. J. G. Jonker,[36] L. Ju,[62] J. Junker,[8,9] C. V. Kalaghatgi,[67] V. Kalogera,[58] B. Kamai,[1] S. Kandhasamy,[84] G. Kang,[37] J. B. Kanner,[1] S. J. Kapadia,[23] S. Karki,[69] K. S. Karvinen,[8,9] R. Kashyap,[16] M. Kasprzack,[1] S. Katsanevas,[28] E. Katsavounidis,[12] W. Katzman,[7] S. Kaufer,[9] K. Kawabe,[44] N. V. Keerthana,[3] F. Kéfélian,[64] D. Keitel,[43] R. Kennedy,[107] J. S. Key,[133] F. Y. Khalili,[61] H. Khan,[26] I. Khan,[14,30] S. Khan,[8,9] Z. Khan,[106] E. A. Khazanov,[134] M. Khursheed,[60] N. Kijbunchoo,[21] Chunglee Kim,[135] J. C. Kim,[136] K. Kim,[90] W. Kim,[54] W. S. Kim,[137] Y.-M. Kim,[138] C. Kimball,[58] E. J. King,[54] P. J. King,[44] M. Kinley-Hanlon,[126] R. Kirchhoff,[8,9] J. S. Kissel,[44] L. Kleybolte,[139] J. H. Klika,[23] S. Klimenko,[47] T. D. Knowles,[38] P. Koch,[8,9] S. M. Koehlenbeck,[8,9] G. Koekoek,[36,140] S. Koley,[36] V. Kondrashov,[1] A. Kontos,[12] N. Koper,[8,9] M. Korobko,[139] W. Z. Korth,[1] I. Kowalska,[73] D. B. Kozak,[1] V. Kringel,[8,9] N. Krishnendu,[141] A. Królak,[142,143] G. Kuehn,[8,9] A. Kumar,[129] P. Kumar,[144] R. Kumar,[106] S. Kumar,[16] L. Kuo,[87] A. Kutynia,[142] S. Kwang,[23] B. D. Lackey,[35] K. H. Lai,[90] T. L. Lam,[90] M. Landry,[44] B. B. Lane,[12] R. N. Lang,[145] J. Lange,[57] B. Lantz,[48] R. K. Lanza,[12] A. Lartaux-Vollard,[25] P. D. Lasky,[6] M. Laxen,[7] A. Lazzarini,[1] C. Lazzaro,[51] P. Leaci,[112,31] S. Leavey,[8,9] Y. K. Lecoeuche,[44] C. H. Lee,[92] H. K. Lee,[146] H. M. Lee,[147] H. W. Lee,[136] J. Lee,[91] K. Lee,[43] J. Lehmann,[8,9] A. Lenon,[38] N. Leroy,[25] N. Letendre,[32] Y. Levin,[6,97] J. Li,[82] K. J. L. Li,[90] T. G. F. Li,[90] X. Li,[45] F. Lin,[6] F. Linde,[36] S. D. Linker,[110] T. B. Littenberg,[148] J. Liu,[62] X. Liu,[23] R. K. L. Lo,[90,1] N. A. Lockerbie,[24] L. T. London,[67] A. Longo,[149,150] M. Lorenzini,[14,15] V. Loriette,[151] M. Lormand,[7] G. Losurdo,[19] J. D. Lough,[8,9] C. O. Lousto,[57] G. Lovelace,[26] M. E. Lower,[152] H. Lück,[9,8] D. Lumaca,[29,30] A. P. Lundgren,[153] R. Lynch,[12] Y. Ma,[45] R. Macas,[67] S. Macfoy,[24] M. MacInnis,[12] D. M. Macleod,[67] A. Macquet,[64] F. Magaña-Sandoval,[41] L. Magaña Zertuche,[84] R. M. Magee,[86] E. Majorana,[31] I. Maksimovic,[151] A. Malik,[60] N. Man,[64] V. Mandic,[42] V. Mangano,[43]

G. L. Mansell,[44,12] M. Manske,[23,21] M. Mantovani,[28] F. Marchesoni,[49,40] F. Marion,[32] S. Márka,[97] Z. Márka,[97] C. Markakis,[10,17] A. S. Markosyan,[48] A. Markowitz,[1] E. Maros,[1] A. Marquina,[101] S. Marsat,[35] F. Martelli,[71,72] I. W. Martin,[43] R. M. Martin,[34] D. V. Martynov,[11] K. Mason,[12] E. Massera,[107] A. Masserot,[32] T. J. Massinger,[1] M. Masso-Reid,[43] S. Mastrogiovanni,[112,31] A. Matas,[42,35] F. Matichard,[1,12] L. Matone,[97] N. Mavalvala,[12] N. Mazumder,[68] J. J. McCann,[62] R. McCarthy,[44] D. E. McClelland,[21] S. McCormick,[7] L. McCuller,[12] S. C. McGuire,[154] J. McIver,[1] D. J. McManus,[21] T. McRae,[21] S. T. McWilliams,[38] D. Meacher,[86] G. D. Meadors,[6] M. Mehmet,[8,9] A. K. Mehta,[16] J. Meidam,[36] A. Melatos,[96] G. Mendell,[44] R. A. Mercer,[23] L. Mereni,[22] E. L. Merilh,[44] M. Merzougui,[64] S. Meshkov,[1] C. Messenger,[43] C. Messick,[86] R. Metzdorff,[70] P. M. Meyers,[96] H. Miao,[11] C. Michel,[22] H. Middleton,[96] E. E. Mikhailov,[155] L. Milano,[78,5] A. L. Miller,[47] A. Miller,[112,31] M. Millhouse,[52] J. C. Mills,[67] M. C. Milovich-Goff,[110] O. Minazzoli,[64,156] Y. Minenkov,[30] A. Mishkin,[47] C. Mishra,[157] T. Mistry,[107] S. Mitra,[3] V. P. Mitrofanov,[61] G. Mitselmakher,[47] R. Mittleman,[12] G. Mo,[93] D. Moffa,[114] K. Mogushi,[84] S. R. P. Mohapatra,[12] M. Montani,[71,72] C. J. Moore,[10] D. Moraru,[44] G. Moreno,[44] S. Morisaki,[81] B. Mours,[32] C. M. Mow-Lowry,[11] Arunava Mukherjee,[8,9] D. Mukherjee,[23] S. Mukherjee,[103] N. Mukund,[3] A. Mullavey,[7] J. Munch,[54] E. A. Muñiz,[41] M. Muratore,[33] P. G. Murray,[43] A. Nagar,[85,158,159] I. Nardecchia,[29,30] L. Naticchioni,[112,31] R. K. Nayak,[160] J. Neilson,[110] G. Nelemans,[63,36] T. J. N. Nelson,[7] M. Nery,[8,9] A. Neunzert,[125] K. Y. Ng,[12] S. Ng,[54] P. Nguyen,[69] D. Nichols,[127,36] S. Nissanke,[127,36] F. Nocera,[28] C. North,[67] L. K. Nuttall,[153] M. Obergaulinger,[20] J. Oberling,[44] B. D. O'Brien,[47] G. D. O'Dea,[110] G. H. Ogin,[161] J. J. Oh,[137] S. H. Oh,[137] F. Ohme,[8,9] H. Ohta,[81] M. A. Okada,[13] M. Oliver,[98] P. Oppermann,[8,9] Richard J. Oram,[7] B. O'Reilly,[7] R. G. Ormiston,[42] L. F. Ortega,[47] R. O'Shaughnessy,[57] S. Ossokine,[35] D. J. Ottaway,[54] H. Overmier,[7] B. J. Owen,[83] A. E. Pace,[86] G. Pagano,[18,19] M. A. Page,[62] A. Pai,[121] S. A. Pai,[60] J. R. Palamos,[69] O. Palashov,[134] C. Palomba,[31] A. Pal-Singh,[139] Huang-Wei Pan,[87] B. Pang,[45] P. T. H. Pang,[90] C. Pankow,[58] F. Pannarale,[112,31] B. C. Pant,[60] F. Paoletti,[19] A. Paoli,[28] A. Parida,[3] W. Parker,[7,154] D. Pascucci,[43] A. Pasqualetti,[28] R. Passaquieti,[18,19] D. Passuello,[19] M. Patil,[143] B. Patricelli,[18,19] B. L. Pearlstone,[43] C. Pedersen,[67] M. Pedraza,[1] R. Pedurand,[22,162] A. Pele,[7] S. Penn,[163] C. J. Perez,[44] A. Perreca,[111,95] H. P. Pfeiffer,[35,117] M. Phelps,[8,9] K. S. Phukon,[3] O. J. Piccinni,[112,31] M. Pichot,[64] F. Piergiovanni,[71,72] G. Pillant,[28] L. Pinard,[22] M. Pirello,[44] M. Pitkin,[43] R. Poggiani,[18,19] D. Y. T. Pong,[90] S. Ponrathnam,[3] P. Popolizio,[28] E. K. Porter,[27] J. Powell,[152] A. K. Prajapati,[106] J. Prasad,[3] K. Prasai,[48] R. Prasanna,[129] G. Pratten,[98] T. Prestegard,[23] S. Privitera,[35] G. A. Prodi,[111,95] L. G. Prokhorov,[61] O. Puncken,[8,9] M. Punturo,[40] P. Puppo,[31] M. Pürrer,[35] H. Qi,[23] V. Quetschke,[103] P. J. Quinonez,[33] E. A. Quintero,[1] R. Quitzow-James,[69] F. J. Raab,[44] H. Radkins,[44] N. Radulescu,[64] P. Raffai,[105] S. Raja,[60] C. Rajan,[60] B. Rajbhandari,[83] M. Rakhmanov,[103] K. E. Ramirez,[103] A. Ramos-Buades,[98] Javed Rana,[3] K. Rao,[58] P. Rapagnani,[112,31] V. Raymond,[67] M. Razzano,[18,19] J. Read,[26] T. Regimbau,[32] L. Rei,[59] S. Reid,[24] D. H. Reitze,[1,47] W. Ren,[17] F. Ricci,[112,31] C. J. Richardson,[33] J. W. Richardson,[1] P. M. Ricker,[17] K. Riles,[125] M. Rizzo,[58] N. A. Robertson,[1,43] R. Robie,[43] F. Robinet,[25] A. Rocchi,[30] L. Rolland,[32] J. G. Rollins,[1] V. J. Roma,[69] M. Romanelli,[66] J. D. Romano,[83] R. Romano,[4,5] C. L. Romel,[44] J. H. Romie,[7] K. Rose,[114] D. Rosińska,[164,53] S. G. Rosofsky,[17] M. P. Ross,[165] S. Rowan,[43] A. Rüdiger,[8,9,‡] P. Ruggi,[28] G. Rutins,[166] K. Ryan,[44] S. Sachdev,[1] T. Sadecki,[44] M. Sakellariadou,[131] L. Salconi,[28] M. Saleem,[141] A. Samajdar,[36] L. Sammut,[6] E. J. Sanchez,[1] L. E. Sanchez,[1] N. Sanchis-Gual,[20] V. Sandberg,[44] J. R. Sanders,[41] K. A. Santiago,[34] N. Sarin,[6] B. Sassolas,[22] P. R. Saulson,[41] O. Sauter,[125] R. L. Savage,[44] P. Schale,[69] M. Scheel,[45] J. Scheuer,[58] P. Schmidt,[63] R. Schnabel,[139] R. M. S. Schofield,[69] A. Schönbeck,[139] E. Schreiber,[8,9] B. W. Schulte,[8,9] B. F. Schutz,[67] S. G. Schwalbe,[33] J. Scott,[43] S. M. Scott,[21] E. Seidel,[17] D. Sellers,[7] A. S. Sengupta,[167] N. Sennett,[35] D. Sentenac,[28] V. Sequino,[29,30,14] A. Sergeev,[134] Y. Setyawati,[8,9] D. A. Shaddock,[21] T. Shaffer,[44] M. S. Shahriar,[58] M. B. Shaner,[110] L. Shao,[35] P. Sharma,[60] P. Shawhan,[75] H. Shen,[17] R. Shink,[168] D. H. Shoemaker,[12] D. M. Shoemaker,[76] S. ShyamSundar,[60] K. Siellez,[76] M. Sieniawska,[53] D. Sigg,[44] A. D. Silva,[13] L. P. Singer,[79] N. Singh,[73] A. Singhal,[14,31] A. M. Sintes,[98] S. Sitmukhambetov,[103] V. Skliris,[67] B. J. J. Slagmolen,[21] T. J. Slaven-Blair,[62] J. R. Smith,[26] R. J. E. Smith,[6] S. Somala,[169] E. J. Son,[137] B. Sorazu,[43] F. Sorrentino,[59] T. Souradeep,[3] E. Sowell,[83] A. P. Spencer,[43] A. K. Srivastava,[106] V. Srivastava,[41] K. Staats,[58] C. Stachie,[64] M. Standke,[8,9] D. A. Steer,[27] M. Steinke,[8,9] J. Steinlechner,[139,43] S. Steinlechner,[139] D. Steinmeyer,[8,9] S. P. Stevenson,[152] D. Stocks,[48] R. Stone,[103] D. J. Stops,[11] K. A. Strain,[43] G. Stratta,[71,72] S. E. Strigin,[61] A. Strunk,[44] R. Sturani,[170] A. L. Stuver,[171] V. Sudhir,[12] T. Z. Summerscales,[172] L. Sun,[1] S. Sunil,[106] J. Suresh,[3] P. J. Sutton,[67] B. L. Swinkels,[36] M. J. Szczepańczyk,[33] M. Tacca,[36] S. C. Tait,[43] C. Talbot,[6] D. Talukder,[69] D. B. Tanner,[47] M. Tápai,[122] A. Taracchini,[35] J. D. Tasson,[93] R. Taylor,[1] F. Thies,[8,9] M. Thomas,[7] P. Thomas,[44] S. R. Thondapu,[60] K. A. Thorne,[7] E. Thrane,[6] Shubhanshu Tiwari,[111,95] Srishti Tiwari,[123] V. Tiwari,[67] K. Toland,[43] M. Tonelli,[18,19] Z. Tornasi,[43] A. Torres-Forné,[173] C. I. Torrie,[1] D. Töyrä,[11]

F. Travasso,[28,40] G. Traylor,[7] M. C. Tringali,[73] A. Trovato,[27] L. Trozzo,[174,19] R. Trudeau,[1] K. W. Tsang,[36] M. Tse,[12] R. Tso,[45] L. Tsukada,[81] D. Tsuna,[81] D. Tuyenbayev,[103] K. Ueno,[81] D. Ugolini,[175] C. S. Unnikrishnan,[123] A. L. Urban,[2] S. A. Usman,[67] H. Vahlbruch,[9] G. Vajente,[1] G. Valdes,[2] N. van Bakel,[36] M. van Beuzekom,[36] J. F. J. van den Brand,[74,36] C. Van Den Broeck,[36,176] D. C. Vander-Hyde,[41] J. V. van Heijningen,[62] L. van der Schaaf,[36] A. A. van Veggel,[43] M. Vardaro,[50,51] V. Varma,[45] S. Vass,[1] M. Vasúth,[46] A. Vecchio,[11] G. Vedovato,[51] J. Veitch,[43] P. J. Veitch,[54] K. Venkateswara,[165] G. Venugopalan,[1] D. Verkindt,[32] F. Vetrano,[71,72] A. Viceré,[71,72] A. D. Viets,[23] D. J. Vine,[166] J.-Y. Vinet,[64] S. Vitale,[12] T. Vo,[41] H. Vocca,[39,40] C. Vorvick,[44] S. P. Vyatchanin,[61] A. R. Wade,[1] L. E. Wade,[114] M. Wade,[114] R. Walet,[36] M. Walker,[26] L. Wallace,[1] S. Walsh,[23] G. Wang,[14,19] H. Wang,[11] J. Z. Wang,[125] W. H. Wang,[103] Y. F. Wang,[90] R. L. Ward,[21] Z. A. Warden,[33] J. Warner,[44] M. Was,[32] J. Watchi,[99] B. Weaver,[44] L.-W. Wei,[8,9] M. Weinert,[8,9] A. J. Weinstein,[1] R. Weiss,[12] F. Wellmann,[8,9] L. Wen,[62] E. K. Wessel,[17] P. Weßels,[8,9] J. W. Westhouse,[33] K. Wette,[21] J. T. Whelan,[57] B. F. Whiting,[47] C. Whittle,[12] D. M. Wilken,[8,9] D. Williams,[43] A. R. Williamson,[127,36] J. L. Willis,[1] B. Willke,[8,9] M. H. Wimmer,[8,9] W. Winkler,[8,9] C. C. Wipf,[1] H. Wittel,[8,9] G. Woan,[43] J. Woehler,[8,9] J. K. Wofford,[57] J. Worden,[44] J. L. Wright,[43] D. S. Wu,[8,9] D. M. Wysocki,[57] L. Xiao,[1] R. Xu,[104] H. Yamamoto,[1] C. C. Yancey,[75] L. Yang,[113] M. J. Yap,[21] M. Yazback,[47] D. W. Yeeles,[67] Hang Yu,[12] Haocun Yu,[12] S. H. R. Yuen,[90] M. Yvert,[32] A. K. Zadrożny,[103,142] M. Zanolin,[33] T. Zelenova,[28] J.-P. Zendri,[51] M. Zevin,[58] J. Zhang,[62] L. Zhang,[1] T. Zhang,[43] C. Zhao,[62] M. Zhou,[58] Z. Zhou,[58] X. J. Zhu,[6] M. E. Zucker,[1,12] and J. Zweizig[1]

(The LIGO Scientific Collaboration and the Virgo Collaboration)

[1] *LIGO, California Institute of Technology, Pasadena, CA 91125, USA*
[2] *Louisiana State University, Baton Rouge, LA 70803, USA*
[3] *Inter-University Centre for Astronomy and Astrophysics, Pune 411007, India*
[4] *Università di Salerno, Fisciano, I-84084 Salerno, Italy*
[5] *INFN, Sezione di Napoli, Complesso Universitario di Monte S.Angelo, I-80126 Napoli, Italy*
[6] *OzGrav, School of Physics & Astronomy, Monash University, Clayton 3800, Victoria, Australia*
[7] *LIGO Livingston Observatory, Livingston, LA 70754, USA*
[8] *Max Planck Institute for Gravitational Physics (Albert Einstein Institute), D-30167 Hannover, Germany*
[9] *Leibniz Universität Hannover, D-30167 Hannover, Germany*
[10] *University of Cambridge, Cambridge CB2 1TN, United Kingdom*
[11] *University of Birmingham, Birmingham B15 2TT, United Kingdom*
[12] *LIGO, Massachusetts Institute of Technology, Cambridge, MA 02139, USA*
[13] *Instituto Nacional de Pesquisas Espaciais, 12227-010 São José dos Campos, São Paulo, Brazil*
[14] *Gran Sasso Science Institute (GSSI), I-67100 L'Aquila, Italy*
[15] *INFN, Laboratori Nazionali del Gran Sasso, I-67100 Assergi, Italy*
[16] *International Centre for Theoretical Sciences, Tata Institute of Fundamental Research, Bengaluru 560089, India*
[17] *NCSA, University of Illinois at Urbana-Champaign, Urbana, IL 61801, USA*
[18] *Università di Pisa, I-56127 Pisa, Italy*
[19] *INFN, Sezione di Pisa, I-56127 Pisa, Italy*
[20] *Departamento de Astronomía y Astrofísica, Universitat de València, E-46100 Burjassot, València, Spain*
[21] *OzGrav, Australian National University, Canberra, Australian Capital Territory 0200, Australia*
[22] *Laboratoire des Matériaux Avancés (LMA), CNRS/IN2P3, F-69622 Villeurbanne, France*
[23] *University of Wisconsin-Milwaukee, Milwaukee, WI 53201, USA*
[24] *SUPA, University of Strathclyde, Glasgow G1 1XQ, United Kingdom*
[25] *LAL, Univ. Paris-Sud, CNRS/IN2P3, Université Paris-Saclay, F-91898 Orsay, France*
[26] *California State University Fullerton, Fullerton, CA 92831, USA*
[27] *APC, AstroParticule et Cosmologie, Université Paris Diderot, CNRS/IN2P3, CEA/Irfu, Observatoire de Paris, Sorbonne Paris Cité, F-75205 Paris Cedex 13, France*
[28] *European Gravitational Observatory (EGO), I-56021 Cascina, Pisa, Italy*
[29] *Università di Roma Tor Vergata, I-00133 Roma, Italy*
[30] *INFN, Sezione di Roma Tor Vergata, I-00133 Roma, Italy*
[31] *INFN, Sezione di Roma, I-00185 Roma, Italy*
[32] *Laboratoire d'Annecy de Physique des Particules (LAPP), Univ. Grenoble Alpes, Université Savoie Mont Blanc, CNRS/IN2P3, F-74941 Annecy, France*
[33] *Embry-Riddle Aeronautical University, Prescott, AZ 86301, USA*
[34] *Montclair State University, Montclair, NJ 07043, USA*
[35] *Max Planck Institute for Gravitational Physics (Albert Einstein Institute), D-14476 Potsdam-Golm, Germany*
[36] *Nikhef, Science Park 105, 1098 XG Amsterdam, The Netherlands*
[37] *Korea Institute of Science and Technology Information, Daejeon 34141, South Korea*
[38] *West Virginia University, Morgantown, WV 26506, USA*
[39] *Università di Perugia, I-06123 Perugia, Italy*

[40] *INFN, Sezione di Perugia, I-06123 Perugia, Italy*
[41] *Syracuse University, Syracuse, NY 13244, USA*
[42] *University of Minnesota, Minneapolis, MN 55455, USA*
[43] *SUPA, University of Glasgow, Glasgow G12 8QQ, United Kingdom*
[44] *LIGO Hanford Observatory, Richland, WA 99352, USA*
[45] *Caltech CaRT, Pasadena, CA 91125, USA*
[46] *Wigner RCP, RMKI, H-1121 Budapest, Konkoly Thege Miklós út 29-33, Hungary*
[47] *University of Florida, Gainesville, FL 32611, USA*
[48] *Stanford University, Stanford, CA 94305, USA*
[49] *Università di Camerino, Dipartimento di Fisica, I-62032 Camerino, Italy*
[50] *Università di Padova, Dipartimento di Fisica e Astronomia, I-35131 Padova, Italy*
[51] *INFN, Sezione di Padova, I-35131 Padova, Italy*
[52] *Montana State University, Bozeman, MT 59717, USA*
[53] *Nicolaus Copernicus Astronomical Center, Polish Academy of Sciences, 00-716, Warsaw, Poland*
[54] *OzGrav, University of Adelaide, Adelaide, South Australia 5005, Australia*
[55] *Theoretisch-Physikalisches Institut, Friedrich-Schiller-Universität Jena, D-07743 Jena, Germany*
[56] *INFN, Sezione di Milano Bicocca, Gruppo Collegato di Parma, I-43124 Parma, Italy*
[57] *Rochester Institute of Technology, Rochester, NY 14623, USA*
[58] *Center for Interdisciplinary Exploration & Research in Astrophysics (CIERA), Northwestern University, Evanston, IL 60208, USA*
[59] *INFN, Sezione di Genova, I-16146 Genova, Italy*
[60] *RRCAT, Indore, Madhya Pradesh 452013, India*
[61] *Faculty of Physics, Lomonosov Moscow State University, Moscow 119991, Russia*
[62] *OzGrav, University of Western Australia, Crawley, Western Australia 6009, Australia*
[63] *Department of Astrophysics/IMAPP, Radboud University Nijmegen, P.O. Box 9010, 6500 GL Nijmegen, The Netherlands*
[64] *Artemis, Université Côte d'Azur, Observatoire Côte d'Azur, CNRS, CS 34229, F-06304 Nice Cedex 4, France*
[65] *Physik-Institut, University of Zurich, Winterthurerstrasse 190, 8057 Zurich, Switzerland*
[66] *Univ Rennes, CNRS, Institut FOTON - UMR6082, F-3500 Rennes, France*
[67] *Cardiff University, Cardiff CF24 3AA, United Kingdom*
[68] *Washington State University, Pullman, WA 99164, USA*
[69] *University of Oregon, Eugene, OR 97403, USA*
[70] *Laboratoire Kastler Brossel, Sorbonne Université, CNRS, ENS-Université PSL, Collège de France, F-75005 Paris, France*
[71] *Università degli Studi di Urbino 'Carlo Bo,' I-61029 Urbino, Italy*
[72] *INFN, Sezione di Firenze, I-50019 Sesto Fiorentino, Firenze, Italy*
[73] *Astronomical Observatory Warsaw University, 00-478 Warsaw, Poland*
[74] *VU University Amsterdam, 1081 HV Amsterdam, The Netherlands*
[75] *University of Maryland, College Park, MD 20742, USA*
[76] *School of Physics, Georgia Institute of Technology, Atlanta, GA 30332, USA*
[77] *Université Claude Bernard Lyon 1, F-69622 Villeurbanne, France*
[78] *Università di Napoli 'Federico II,' Complesso Universitario di Monte S.Angelo, I-80126 Napoli, Italy*
[79] *NASA Goddard Space Flight Center, Greenbelt, MD 20771, USA*
[80] *Dipartimento di Fisica, Università degli Studi di Genova, I-16146 Genova, Italy*
[81] *RESCEU, University of Tokyo, Tokyo, 113-0033, Japan.*
[82] *Tsinghua University, Beijing 100084, China*
[83] *Texas Tech University, Lubbock, TX 79409, USA*
[84] *The University of Mississippi, University, MS 38677, USA*
[85] *Museo Storico della Fisica e Centro Studi e Ricerche "Enrico Fermi", I-00184 Roma, Italyrico Fermi, I-00184 Roma, Italy*
[86] *The Pennsylvania State University, University Park, PA 16802, USA*
[87] *National Tsing Hua University, Hsinchu City, 30013 Taiwan, Republic of China*
[88] *Charles Sturt University, Wagga Wagga, New South Wales 2678, Australia*
[89] *University of Chicago, Chicago, IL 60637, USA*
[90] *The Chinese University of Hong Kong, Shatin, NT, Hong Kong*
[91] *Seoul National University, Seoul 08826, South Korea*
[92] *Pusan National University, Busan 46241, South Korea*
[93] *Carleton College, Northfield, MN 55057, USA*
[94] *INAF, Osservatorio Astronomico di Padova, I-35122 Padova, Italy*
[95] *INFN, Trento Institute for Fundamental Physics and Applications, I-38123 Povo, Trento, Italy*
[96] *OzGrav, University of Melbourne, Parkville, Victoria 3010, Australia*
[97] *Columbia University, New York, NY 10027, USA*
[98] *Universitat de les Illes Balears, IAC3—IEEC, E-07122 Palma de Mallorca, Spain*

[99] *Université Libre de Bruxelles, Brussels 1050, Belgium*
[100] *Sonoma State University, Rohnert Park, CA 94928, USA*
[101] *Departamento de Matemáticas, Universitat de València, E-46100 Burjassot, València, Spain*
[102] *University of Rhode Island, Kingston, RI 02881, USA*
[103] *The University of Texas Rio Grande Valley, Brownsville, TX 78520, USA*
[104] *Bellevue College, Bellevue, WA 98007, USA*
[105] *MTA-ELTE Astrophysics Research Group, Institute of Physics, Eötvös University, Budapest 1117, Hungary*
[106] *Institute for Plasma Research, Bhat, Gandhinagar 382428, India*
[107] *The University of Sheffield, Sheffield S10 2TN, United Kingdom*
[108] *IGFAE, Campus Sur, Universidade de Santiago de Compostela, 15782 Spain*
[109] *Dipartimento di Scienze Matematiche, Fisiche e Informatiche, Università di Parma, I-43124 Parma, Italy*
[110] *California State University, Los Angeles, 5151 State University Dr, Los Angeles, CA 90032, USA*
[111] *Università di Trento, Dipartimento di Fisica, I-38123 Povo, Trento, Italy*
[112] *Università di Roma 'La Sapienza,' I-00185 Roma, Italy*
[113] *Colorado State University, Fort Collins, CO 80523, USA*
[114] *Kenyon College, Gambier, OH 43022, USA*
[115] *Christopher Newport University, Newport News, VA 23606, USA*
[116] *National Astronomical Observatory of Japan, 2-21-1 Osawa, Mitaka, Tokyo 181-8588, Japan*
[117] *Canadian Institute for Theoretical Astrophysics, University of Toronto, Toronto, Ontario M5S 3H8, Canada*
[118] *Observatori Astronòmic, Universitat de València, E-46980 Paterna, València, Spain*
[119] *School of Mathematics, University of Edinburgh, Edinburgh EH9 3FD, United Kingdom*
[120] *Institute Of Advanced Research, Gandhinagar 382426, India*
[121] *Indian Institute of Technology Bombay, Powai, Mumbai 400 076, India*
[122] *University of Szeged, Dóm tér 9, Szeged 6720, Hungary*
[123] *Tata Institute of Fundamental Research, Mumbai 400005, India*
[124] *INAF, Osservatorio Astronomico di Capodimonte, I-80131, Napoli, Italy*
[125] *University of Michigan, Ann Arbor, MI 48109, USA*
[126] *American University, Washington, D.C. 20016, USA*
[127] *GRAPPA, Anton Pannekoek Institute for Astronomy and Institute of High-Energy Physics, University of Amsterdam, Science Park 904, 1098 XH Amsterdam, The Netherlands*
[128] *Delta Institute for Theoretical Physics, Science Park 904, 1090 GL Amsterdam, The Netherlands*
[129] *Directorate of Construction, Services & Estate Management, Mumbai 400094 India*
[130] *University of Białystok, 15-424 Białystok, Poland*
[131] *King's College London, University of London, London WC2R 2LS, United Kingdom*
[132] *University of Southampton, Southampton SO17 1BJ, United Kingdom*
[133] *University of Washington Bothell, Bothell, WA 98011, USA*
[134] *Institute of Applied Physics, Nizhny Novgorod, 603950, Russia*
[135] *Ewha Womans University, Seoul 03760, South Korea*
[136] *Inje University Gimhae, South Gyeongsang 50834, South Korea*
[137] *National Institute for Mathematical Sciences, Daejeon 34047, South Korea*
[138] *Ulsan National Institute of Science and Technology, Ulsan 44919, South Korea*
[139] *Universität Hamburg, D-22761 Hamburg, Germany*
[140] *Maastricht University, P.O. Box 616, 6200 MD Maastricht, The Netherlands*
[141] *Chennai Mathematical Institute, Chennai 603103, India*
[142] *NCBJ, 05-400 Świerk-Otwock, Poland*
[143] *Institute of Mathematics, Polish Academy of Sciences, 00656 Warsaw, Poland*
[144] *Cornell University, Ithaca, NY 14850, USA*
[145] *Hillsdale College, Hillsdale, MI 49242, USA*
[146] *Hanyang University, Seoul 04763, South Korea*
[147] *Korea Astronomy and Space Science Institute, Daejeon 34055, South Korea*
[148] *NASA Marshall Space Flight Center, Huntsville, AL 35811, USA*
[149] *Dipartimento di Matematica e Fisica, Università degli Studi Roma Tre, I-00146 Roma, Italy*
[150] *INFN, Sezione di Roma Tre, I-00146 Roma, Italy*
[151] *ESPCI, CNRS, F-75005 Paris, France*
[152] *OzGrav, Swinburne University of Technology, Hawthorn VIC 3122, Australia*
[153] *University of Portsmouth, Portsmouth, PO1 3FX, United Kingdom*
[154] *Southern University and A&M College, Baton Rouge, LA 70813, USA*
[155] *College of William and Mary, Williamsburg, VA 23187, USA*
[156] *Centre Scientifique de Monaco, 8 quai Antoine Ier, MC-98000, Monaco*
[157] *Indian Institute of Technology Madras, Chennai 600036, India*
[158] *INFN Sezione di Torino, Via P. Giuria 1, I-10125 Torino, Italy*
[159] *Institut des Hautes Etudes Scientifiques, F-91440 Bures-sur-Yvette, France*
[160] *IISER-Kolkata, Mohanpur, West Bengal 741252, India*

[161] *Whitman College, 345 Boyer Avenue, Walla Walla, WA 99362 USA*

[162] *Université de Lyon, F-69361 Lyon, France*

[163] *Hobart and William Smith Colleges, Geneva, NY 14456, USA*

[164] *Janusz Gil Institute of Astronomy, University of Zielona Góra, 65-265 Zielona Góra, Poland*

[165] *University of Washington, Seattle, WA 98195, USA*

[166] *SUPA, University of the West of Scotland, Paisley PA1 2BE, United Kingdom*

[167] *Indian Institute of Technology, Gandhinagar Ahmedabad Gujarat 382424, India*

[168] *Université de Montréal/Polytechnique, Montreal, Quebec H3T 1J4, Canada*

[169] *Indian Institute of Technology Hyderabad, Sangareddy, Khandi, Telangana 502285, India*

[170] *International Institute of Physics, Universidade Federal do Rio Grande do Norte, Natal RN 59078-970, Brazil*

[171] *Villanova University, 800 Lancaster Ave, Villanova, PA 19085, USA*

[172] *Andrews University, Berrien Springs, MI 49104, USA*

[173] *Max Planck Institute for Gravitationalphysik (Albert Einstein Institute), D-14476 Potsdam-Golm, Germany*

[174] *Università di Siena, I-53100 Siena, Italy*

[175] *Trinity University, San Antonio, TX 78212, USA*

[176] *Van Swinderen Institute for Particle Physics and Gravity, University of Groningen, Nijenborgh 4, 9747 AG Groningen, The Netherlands*

(Dated: July 17, 2019)

---

* Deceased, February 2018.

† Deceased, November 2017.

‡ Deceased, July 2018.

Supplement To: Directional limits on persistent gravitational waves using data from Advanced LIGO's first two observing runs

(The LIGO Scientific Collaboration and Virgo Collaboration)

In this technical supplement we provide additional formulas to support the main text. This closely follows the discussion given in [11].

Following past analyses, we assume that we can factorize $\Omega_{\rm gw}(f,\Theta)$ into frequency and sky-direction-dependent terms

$$\Omega_{\rm gw}(f,\Theta) = \frac{2\pi^2}{3H_0^2} f^3 H(f) \mathcal{P}(\Theta). \tag{A1}$$

Note that this quantity has units of the dimensionless energy density parameter per steradian. For the radiometer searches it is useful to define a different representation in terms of energy flux,

$$\mathcal{F}(f,\Theta) = \frac{c^3\pi}{4G} f^2 H(f) \mathcal{P}(\Theta), \tag{A2}$$

which has units of $\mathrm{erg\,s^{-1}\,cm^{-2}\,Hz^{-1}\,sr^{-1}}$, where c is the speed of light and G is Newton's gravitational constant.

We use two different representations to estimate the angular power, $\mathcal{P}(\Theta)$. The *radiometer* method [17, 41] (in both the broadband (BBR) and narrowband (NBR) applications) is optimized for a small number of resolvable, separated point sources on the sky, and so we estimate the angular power in terms of point sources by decomposing onto delta functions

$$\mathcal{P}(\Theta) = \mathcal{P}_{\Theta_0} \delta^2(\Theta,\Theta_0). \tag{A3}$$

The radiometer method assumes that the sources are well-localized on the sky (that is, to within one pixel), and so it is not well-suited to sources which are spread over a large solid angle.

To characterize diffuse sources of GWs, we use the *spherical harmonic decomposition* (SHD) [20]. We write the angular power in terms of a sum over spherical harmonics, $Y_{lm}(\Theta)$, with amplitude coefficients, $\mathcal{P}_{lm}$

$$\mathcal{P}(\Theta) = \sum_{l=0}^{l_{\rm max}} \sum_{m=-l}^{l} \mathcal{P}_{lm} Y_{lm}(\Theta). \tag{A4}$$

In principle, $l_{\rm max}$ should be infinite. However in practice, we must take a finite value of $l_{\rm max}$. The optimal choice for $l_{\rm max}$ depends upon the spatial separation and the sensitivity curve of the detectors. We use the same choice as in the previous analysis [11], taking $l_{\rm max} = \{3, 4, 16\}$ for the 3 spectral indices.

By construction, the NBR search looks for signals in a narrow range of frequency bins. On the other hand, for the broadband SHD and BBR searches, we must make an additional assumption about the spectral shape of the source. We assume that the GW power spectrum takes a power-law form,

$$H(f) = \left(\frac{f}{f_{\rm ref}}\right)^{\alpha-3}. \tag{A5}$$

In this case, the power in each direction is characterized by a spectral index, α, and the amplitude of the energy density or flux at a given reference frequency, $f_{\rm ref}$. As described in the main text, we choose $f_{\rm ref} = 25\,\mathrm{Hz}$ and search for and set limits on spectral indices of $\alpha = (0,\, 2/3,\, 3)$.

Given the spectral shape $H(f)$, we define the following quantities which are used to construct the sky maps. For the BBR search it is convenient to consider the flux F_{α,Θ_0},

$$F_{\alpha,\Theta_0} \equiv \int d^2\Theta\, \mathcal{F}(f_{\rm ref},\Theta) = \frac{c^3\pi}{4G} f_{\rm ref}^2 \mathcal{P}_{\Theta_0}. \tag{A6}$$

For the SHD search, we will use the dimensionless energy density per unit sky area

$$\Omega_\alpha(\Theta) \equiv \Omega_{\rm gw}(f_{\rm ref},\Theta) = \frac{2\pi^2}{3H_0^2} f_{\rm ref}^3 \mathcal{P}(\Theta). \tag{A7}$$

For more details, see [11].

The starting point of the stochastic analysis is the cross-correlation function $C(f;t)$, which is given by

$$C(f;t) = \frac{2}{T} \tilde{s}_1^*(f;t) \tilde{s}_2(f;t), \tag{A8}$$

where $s_i(f;t)$ is the Fourier transform of length T of the data from detector i at time t. To produce a sky map, we convolve $C(f,t)$ with the generalized overlap reduction function $\gamma_\mu(f,t)$, which encodes the time delay between the detectors and the detector response (see [20] for an explicit definition). We construct the dirty-map X_μ (see below)

$$X_\mu = \sum_{f,t} \gamma_\mu^*(f,t) \frac{H(f)}{P_1(f;t)P_2(f;t)} C(f;t). \tag{A9}$$

Here, $P_i(f;t)$ is the (one-sided) power spectral density of the noise in detector i and $H(f)$ is the chosen spectral model. We use Greek indices $\mu, \nu, \cdots$ to represent angular degrees of freedom. For the SHD search, μ, ν run over the spherical harmonic coefficients, e.g., $\mu \equiv (lm)$. For the BBR and NBR searches, μ, ν run over individual sky directions (pixels).

The quantity X_μ is called the "dirty map" because it does not faithfully represent the true gravitational-wave

power on the sky. In order to obtain the true power, following [20] we introduce the Fisher information matrix, $\Gamma_{\mu\nu}$, which encodes the beam pattern of the detector network

$$\Gamma_{\mu\nu} = \sum_{f,t} \gamma^*_\mu(f,t) \frac{H^2(f)}{P_1(f;t)P_2(f;t)} \gamma_\nu(f;t). \tag{A10}$$

We can get an estimate of the GW power by inverting the Fisher matrix, $\hat{\mathcal{P}}_{\mu\nu} = \Gamma^{-1}_{\mu\nu} X_\nu$. In the case of the BBR and NBR, we ignore correlations between neighboring pixels, and so we don't perform a full matrix inversion, instead taking the inverse of the diagonal elements of the Fisher matrix:

$$\hat{\mathcal{P}}_\Theta = (\Gamma_{\Theta\Theta})^{-1} X_\Theta, \tag{A11}$$

$$\sigma_\Theta = (\Gamma_{\Theta\Theta})^{-1/2}. \tag{A12}$$

In the case of the spherical harmonics, we formally construct an unbiased estimator of the clean map (i.e., the physical map of GW power) using a maximum likelihood estimator [20]

$$\hat{\mathcal{P}}_{lm} = \sum_{l'm'} [\Gamma^{-1}_{\rm R}]_{lm,l'm'} X_{l'm'}. \tag{A13}$$

The Fisher matrix is degenerate because of the existence of blind spots in the detector network, as well as the diffraction limit, [20]. As a result we need to regularize the Fisher matrix to define an inverse.

Construction of a clean map in the pixel basis, as opposed to the spherical harmonics basis, has been proposed [13, 20, 41] and implemented on O1 data [14]. This method also suffers from a poorly-conditioned Fisher information matrix, but given that it avoids a spherical harmonics decomposition entirely, it does not use an initial cut-off in $l_{\rm max}$ as our search does.